

Jet-Supercavity Interaction: Insights from Experiments

MJ Moeny¹, MH Krane¹, IN Kirschner², MP Kinzel¹

¹ Applied Research Laboratory, The Pennsylvania State University, University Park, PA, USA

² Applied Physical Sciences, Groton, CT, USA

E-mail: mjm369@arl.psu.edu

Abstract. An experimental study was performed to evaluate some of the claims of Paryshev (2006) regarding changes to ventilated cavity behavior caused by the interaction of a jet with the cavity closure region. The experiments, conducted in the 1.22m dia. Garfield Thomas Water Tunnel, were performed for EDD to tunnel diameter of 0.022, $Fr = 14.5$ and 26.2 . The model consisted of a converging-section nozzle mounted to the base of a 27.9mm 37° cone cavitator placed on the tunnel centerline at the end of a 138.4mm long streamlined strut. A ventilated cavity was formed over the model, then an air jet, issuing from a converging nozzle, was initiated. Changes to cavity behavior were quantified in terms of cavitation number, thrust-to-drag ratio, and stagnation pressure ratio at the jet nozzle. The results show that, while the overall trends predicted by Paryshev were observed, the data did not fully collapse, suggesting that many of the effects neglected by Paryshev's model have measureable effect.

1. Introduction

This paper presents an experimental effort to evaluate model predictions of Paryshev (2006), concerning the effect of jet/closure interaction on the behavior of a ventilated cavity. That model was based on several simplifying assumptions, three of which are: (1) the jet is narrow, so the region over which jet/closure interaction occurred is short in the axial direction, (2) the jet does not significantly entrain gas from the ventilated cavity, so that the jet stagnation pressure does not vary over the length of the jet, and (3) the pressure in the ventilated cavity is uniform over the length of the cavity, upstream of the closure region, in which the pressure rises rapidly to stagnation pressure, then falls to ambient pressure at the downstream end of the cavity. Paryshev proposed that the jet/closure interaction, and its effect on the cavity as a whole, are governed by two parameters: $P = \rho_\infty U_\infty^2 / \rho_j U_j^2$, the ratio of the stagnation pressure of the fluid flow outside the cavity to that of the jet, and $\bar{J} = \rho_j U_j^2 S_j / D_n$, the ratio of jet momentum flux to the drag on the cavitator.

The combination of these two parameters determines the effect of the jet on the closure region, as shown in Figure 1. The figure shows \bar{J} vs. P space, with regions colored according to the behavior Paryshev predicted. In the region $P < 1$ (blue in the figure), where the jet stagnation pressure exceeds that of the pressure outside the closure region (roughly, the total pressure of the exterior flow), the jet strongly penetrates the cavity closure region, strongly modifying the closure region dynamics, increasing the rate at which gas leaks from the cavity, resulting in a smaller cavity (higher cavitation number). Paryshev notes the similarity to the *Efros-type closure*. When $P > 1$, jet stagnation pressure is always less than the exterior pressure, and there are two possibilities, depending on the value of the thrust to drag ratio \bar{J} . For low jet thrust, $\bar{J} < 1/2$, the jet effect on the closure region is minimal, and the jet acts to supplement



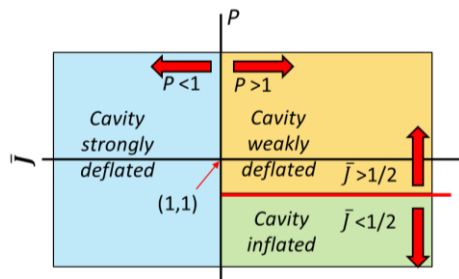


Figure 1. Parameter space describing jet/cavity closure interaction regimes, after Paryshev (2006). $P < 1$ (blue): jet strongly deflates cavity. $P > 1$, $\bar{J} > 1/2$ (orange): jet weakly deflates cavity. $P > 1$, $\bar{J} < 1/2$ (green): jet inflates cavity.

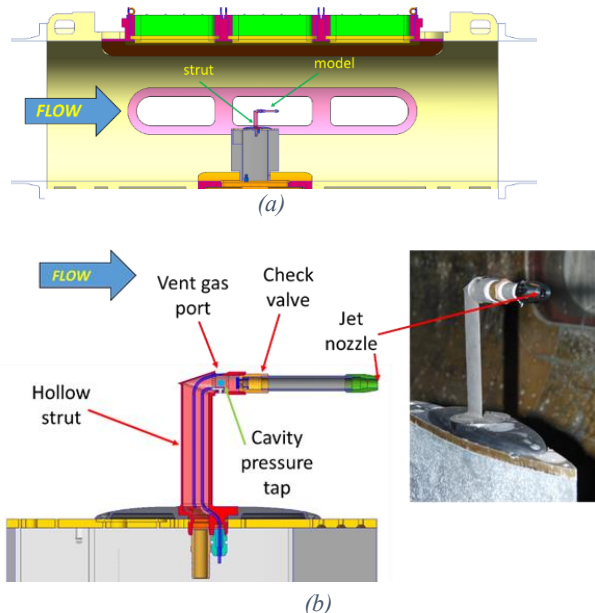


Figure 2. Schematic of experimental setup. (a) model installed in water tunnel test section. (b) Detail of model. Cavitator and strut jet air and cavity ventilation air, as well as the pressure line passed through the strut. A check valve prevented water from leaking back into the jet gas system. Model body consists of a short section of aluminum pipe and a converging nozzle.

valve, then a hollow aluminum cylindrical body (1.52cm OD, 1.27cm ID), and finally an aluminum converging nozzle were attached in series, using standard pipe thread. The cavitator/strut piece was fabricated as one piece from laser-sintered Inconel, permitting the strut to be low-profile and minimizing interference of its attachment to the cavitator. The hollow strut provides passage of (i) ventilation air through a separate line, (ii) a tube connecting the cavity pressure port on the side of the cavitator to a differential pressure transducer located outside the tunnel, and (iii) jet gas air, which flows through the remaining space in the strut. Two separate bottled high-pressure dry air reservoirs supplied air, one each to the cavity ventilation and to the jet.

2.2 Measurements

A differential pressure sensor connected between the cavity pressure tap on the cavitator and to the tunnel wall at the same axial location as the model, measured Δp_{cav} , the difference between cavity and tunnel static pressure. Also measured were ventilation gas mass flow rate and jet gas mass flow rate

cavity ventilation, enlarging the cavity (reducing cavitation number). As thrust increases to $\bar{J} > 1/2$, the jet more strongly modifies the closure region, though not as severely as when $P < 1$, increasing the gas leakage rate, and reducing the cavity size (increasing cavitation number).

As noted, Paryshev's model contained strong simplifications, and its predictions were compared to only a single data set, about which not much detail was given. The experiments reported here, and the parallel low-order modeling (Kirschner, *et al.*, 2015, these proceedings) and computer simulation (Kinzel, *et al.*, 2015, these proceedings) efforts were therefore undertaken to test the extent to which the behavior predicted by Paryshev's model can be observed.

2. Methods

Experiments were conducted in the (1.22m) diameter Garfield Thomas Water Tunnel (see, *e.g.*, Lehman, 1959; Marboe, *et al.*, 1993) at the Penn State University Applied Research Laboratory. The closed-loop tunnel features a 4.27m long test section in which tunnel speed can be varied continuously from approximately 1 to 16m/s with independent control of test section static pressure from 14kPa to 414kPa absolute over the full velocity range.

2.1 Physical Model

The experimental setup is shown in Figure 2. Figure 2a shows the model installed in the GTWT, while Figure 2b shows a detail of the model. The model consists of a strut based on a NACA 16-0021 foil of 3.51cm chord x 0.66 cm thickness and in one piece with conical cavitator, base diameter $d_n = 2.79$ cm, with a 37° included angle. Comparing the calculated C_D of this cone to that of an equivalent flat disk and the water tunnel gives a ratio of equivalent disk diameter (EDD) to tunnel diameter of 0.022. Moving downstream from the base of the cone, a check

using two thermal mass flow meters, jet gas reservoir and tunnel water temperatures using two resistance temperature detectors, and tunnel total pressure and tunnel static pressure at discrete axial locations through the test section using multiple gage-pressure sensors. Finally, a high-speed digital video camera was used to acquire video images of the cavity at a rate of 1500 frames/s.

Measured differential cavity pressure and calculated tunnel flow velocity and density were used to estimate the cavitation number, $\sigma = 2\Delta p_{cav} / \rho_{\infty} U_{\infty}^2$. The jet gas line measurements, cavity pressure and tunnel pressure were used to iteratively estimate jet gas reservoir pressure just upstream of the nozzle, along with jet speed and Mach number, as well as momentum flux at the nozzle. These were used to estimate the cavitator drag coefficient $C_d = 0.21 + 0.546\sigma$, using data from May (1975). The above quantities then returned \bar{J} and P for each case measured.

3. Results

3.1 Cases studied

Each measurement consisted of establishing an over-ventilated cavity, and then introducing the jet at a target flow rate. Data was collected at two tunnel speeds, $U_{\infty} = 7.62\text{m/s}$ and 13.7m/s , corresponding to Froude numbers $Fr = U_{\infty}/(g d_n)^{1/2}$ equal to 14.5 and 26.2, respectively, and for two nozzle diameters, 7mm and 11mm. Target nondimensional ventilation flow rates $C_Q = Q/(U_{\infty} d_n^2)$ were $C_Q = 7$ for $Fr = 14.5$, and $C_Q = 15$ for $Fr = 26.2$. Jet mass flow rates varied from 0 to 0.11kg/s. These correspond, for the two nozzles, to a jet momentum flux range of 0 to 12N.

The ranges of momentum flux, measured cavitation number, and tunnel flow speed combine to define the ranges of the two control parameters, \bar{J} and P , identified by Paryshev, as shown in Figure 3. According to the predictions, the regime map shows that as jet momentum is increased the 7mm nozzle jet first induces cavity inflation at low jet thrust, then strong deflation beginning near $\bar{J} \approx 1/2$, $P \approx 1$. Behavior for the 11mm nozzle jet is more complex. As thrust increases, the cavity should transition from inflation to weak deflation at $\bar{J} \approx 1/2$, $P \approx 2.2$, then from weak inflation to strong deflation at $\bar{J} \approx 1$, $P \approx 1$. Experimental data overlaid on the regime map shows all three regimes are represented.

3.2 Observed changes to cavity behavior due to jet

Figure 4 shows still images from the high-speed video for cases where a stable cavity was formed. In the figure, P and \bar{J} vary in the vertical direction, while P is approximately constant horizontally. The left column contains 7mm jet nozzle data while the right column contains 11mm jet nozzle data. As discussed above, cavity size can be seen to vary with increasing \bar{J} . For the 7mm nozzle, data showed a maximum diameter near

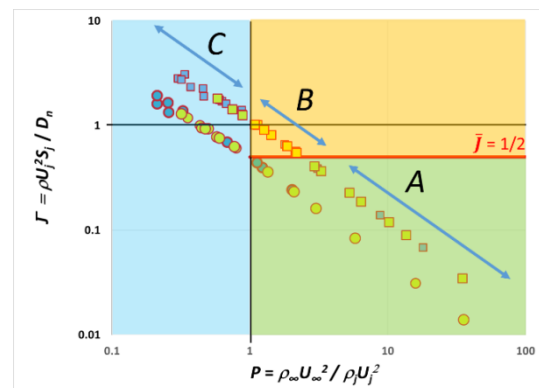


Figure 3. Jet/closure interaction regime map overlaid with values corresponding to measured data; jet/closure interaction regimes colored as in Figure 1. Nozzle diameter: $\circ = 7\text{mm}$, $\square = 11\text{mm}$. $Fr = 14.5$ (dark/blue fill), $Fr = 26.2$ (light/yellow fill). Data group by nozzle dia. Jet acts to A: inflate cavity, B: weakly deflate cavity, C: strongly deflate cavity.

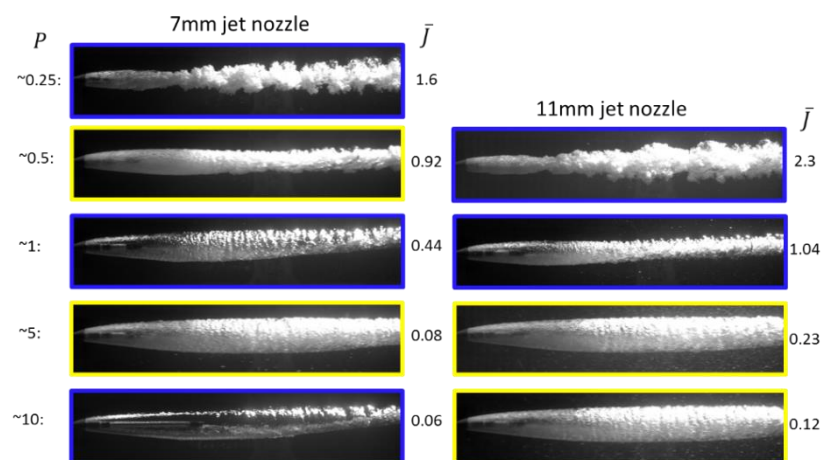


Figure 4. Cavity size trends, still images from high-speed video. Images at same level occurred at approximately same value of P , indicated to the left. Corresponding values of \bar{J} are given to the right of each image. Image border color indicates tunnel flow speed – dark/blue: $Fr = 14.5$, light/yellow: $Fr = 26.2$.

$\bar{J} \approx 1/2$, $P \approx 1$, as illustrated by the image for $\bar{J} = 0.44$. The maximum cavity size for the 11mm nozzle appears to occur in the range $1 < P < 5$, $0.23 < \bar{J} < 1$. For both nozzles, cavity size decreases strongly with \bar{J} for $P < 1$.

Figure 5 shows cavitation number, σ (essentially inversely proportional to cavity size), plotted against both P and \bar{J} . Figure 4a shows that, for decreasing P , σ does not vary strongly until $P \approx 2$ for the 11mm nozzle, and until $P \approx 1$ for the 7mm nozzle. After these points, σ rises rapidly with P . Figure 4b shows that, for increasing \bar{J} , σ does not vary strongly until $\bar{J} \approx 0.6$, at which point it rises rapidly. Furthermore, data show a larger σ variation for $\bar{J} > 0.6$. It should be noted that in both Fig. 4a and 4b, the highest σ cases correspond to situations where the cavity completely collapsed due to jet action. Finally, behavior for $\bar{J} < 1/2$ appears at some variance with Paryshev's model. Cavitation number appears to reach a weak minimum at low \bar{J} , but, for all but one case, it occurs for $\bar{J} \ll 1/2$, and does not coincide to the rapid rise in cavitation number with \bar{J} observed near $\bar{J} \approx 1/2$.

4. Discussion

Principle predicted trends were observed: regime change was observed for $P \approx 1$, $\bar{J} \approx 1$, and also at $P > 1$, $\bar{J} \approx 1/2$, though regime boundaries are not precise and appear to be dependent on jet nozzle diameter and Fr . It is speculated that physical phenomena neglected in the approximate model, especially jet entrainment, are responsible for these variations, though it should be admitted that the current data cover only a small portion of the weak deflation

($P > 1$, $\bar{J} > 1/2$) regime.

5. Summary and Conclusions

An experimental investigation was performed to test some of the predictions of the jet/closure interaction model described by Paryshev (2006). The principle predicted trends were observed, but differences motivate further study to account for the influence of effects neglected in the analysis.

Acknowledgments

The authors gratefully acknowledge funding through ONR Grant Numbers N00014-12-1-0489 and N00014-13-1-0692, Dr. Ronald Joslin, Program Manager.

References

- Lehman AF 1959 The Garfield Thomas Water Tunnel ARL Penn State Technical Report No. NOrd 16597-56.
- Marboe R C Weyer RM and Jonson ML 1993 Hydroacoustic Research capabilities in the Large Water Tunnel at ARL-Penn State NCA-VOL 15/FED **168** pp. 125-135.
- May A 1975 Water Entry and Cavity-Running Behavior of Missiles Naval Sea Systems Command Tech. Rep. SEAHAC/TR 75-2.
- Paryshev EV 2006 Approximate mathematical models in high-speed hydrodynamics *J. Eng. Math.* **55** pp 41-64.

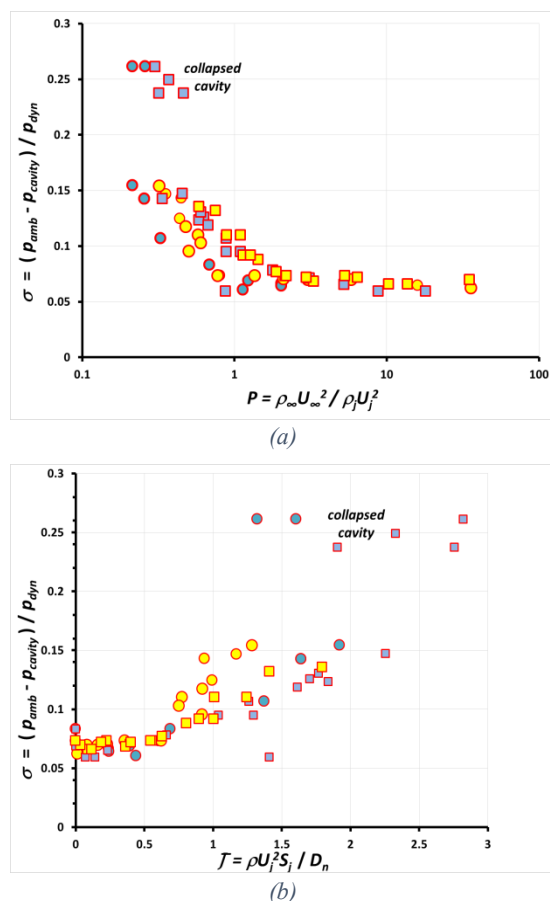


Figure 5. Cavitation number as function of (a) stagnation pressure ratio P , (b) thrust to drag ratio \bar{J} and \circ - 7mm nozzle diameter, \square - 11mm nozzle diameter, dark/blue fill - $Fr = 14.5$, light/yellow fill - $Fr = 26.2$.